Research Article | Vol. 28, No. 22 / 26 October 2020 / Optics Express 33307
Optics EXPRESS

Gain-switched semiconductor lasers with pulsed excitation and optical injection for dual-comb spectroscopy

C. QUEVEDO-GALÁN,[1,*] V. DURÁN,[2] A. ROSADO,[1] A. PÉREZ-SERRANO,[1] J. M. G. TIJERO,[1] AND I. ESQUIVIAS[1]

[1] CEMDATIC - E.T.S.I. Telecomunicación, Universidad Politécnica de Madrid (UPM), 28040 Madrid, Spain
[2] GROC-UJI, Institute of New Imaging Technologies (INIT), Universitat Jaume I, 12071 Castellón, Spain
[*] clara.quevedo.galan@upm.es

Abstract: In this work we demonstrate the capability of two gain-switched optically injected semiconductor lasers to perform high-resolution dual-comb spectroscopy. The use of low duty cycle pulse trains to gain switch the lasers, combined with optical injection, allows us to obtain flat-topped optical frequency combs with 350 optical lines (within 10 dB) spaced by 100 MHz. These frequency combs significantly improve the spectral resolution reported so far on dual-comb spectroscopy with gain-switched laser diodes. We evaluate the performance of our system by measuring the transmission profile of an absorption line of $H^{13}CN$ at the C-band, analyzing the attainable signal-to-noise ratio for a range of averaging times.

© 2020 Optical Society of America under the terms of the OSA Open Access Publishing Agreement

1. Introduction

Since the beginning of the century, optical frequency comb (OFC) technology has revolutionized the field of optical metrology [1–3], finding applications in a plethora of fields, including molecular spectroscopy, telecommunications, astronomy and remote sensing, to cite just a few [4–8]. In parallel to the search for innovative applications, many efforts have been devoted to develop alternatives to mode-locked OFCs, with the aim of providing tunable, cost-efficient and field-deployable comb generators [9–11]. Among these comb platforms, OFCs generated from semiconductor lasers by gain-switching (GS) have attracted considerable attention in recent years [12–26]. Besides benefiting from the usual advantages of semiconductor sources (high efficiency, low cost and small footprint), the comb generation by GS also offers low losses, flexible comb line spacing and, outstandingly, suitability for photonic integration [20]. OFCs based on GS have been applied in optical communications [21,22], sub-terahertz generation [23,27] and dual-comb spectroscopy (DCS) [16,24].

DCS is a well-established technique that provides fast and accurate spectroscopic measurements by using low-bandwidth electronics, thanks to an efficient down-conversion of the optical frequencies into the radio-frequency (RF) domain [28]. In order to benefit from the outstanding capabilities of DCS, a high degree of mutual coherence is required between two individual combs. This requirement can be accomplished by the generation of a couple of optical combs from a single laser cavity, since common-noise cancellation avoids the need of sophisticated phase-locking methods [29–33]. Thus, a Kerr-lens mode-locked bidirectional ring laser enables the generation of two combs with slightly different line spacing, due to the asymmetry between the clockwise and counterclockwise directions [29]. Around 1 μm, an all-polarization-maintaining dual-color ytterbium fiber laser can be used, for instance, as a dual-comb generator [30]. In this case, the generated train of pulses has separated central wavelengths, so spectral overlap requires nonlinear spectral broadening of one of the combs. In the same spectral window, mode-locked integrated external-cavity surface emitting lasers constitute a very compact design to carry out DCS with picosecond [31,32] or femtosecond [33] optical pulses. However, in frequency combs

#404398 https://doi.org/10.1364/OE.404398
Journal © 2020 Received 5 Aug 2020; revised 25 Sep 2020; accepted 25 Sep 2020; published 21 Oct 2020

Optics EXPRESS

based on laser cavities, the pulse repetition rate (and therefore the comb spacing) is set by the cavity length. In contrast, combs generated by GS of semiconductor lasers feature optical spectra with a line spacing that can be electronically reconfigured, in principle over orders of magnitude. Additionally, when applied to DCS, gain-switched OFCs offer simple and tunable control of the difference between the line spacing of the combs, no need of nonlinear broadening to ensure comb overlap and a potential implementation from visible to mid-infrared [24].

The usual manner of generating OFCs by GS consists in driving a semiconductor laser by a bias current plus a RF sinusoidal current. In this scheme, the frequency and amplitude of the sinusoidal signal, as well as the bias value, constitute the set of parameters that determines the comb generation process. A systematic analysis of the effect of the switching conditions on the performance of the OFCs was reported in [26]. Briefly, for repetition frequencies of the order of the frequency of the laser relaxation oscillations (roughly ~5-25 GHz), the GS mechanism produces a broad spectrum with well-defined spectral lines. In the time domain, the result is a train of optical pulses, whose coherence has demonstrated to be effectively preserved with optical injection (OI) from a master laser to a slave gain-switched laser [14]. Using this scheme, and for repetition rates >5 GHz, high-quality flat combs can be produced by a proper adjustment of the switching and OI parameters [12,15]. Beyond comb generation, the OI technique also plays an important role in the implementation of DCS systems, since the use of a single master laser ensures a high degree of mutual coherence between two gain-switched OFCs with different line spacing [16,24].

As demonstrated in [26], for repetition frequencies <1 GHz the range of driving conditions to generate broad and flat-topped OFCs under sinusoidal GS is dramatically reduced. In addition, the quality of the OFCs cannot be significantly improved by OI. This fact sets a limit to the maximum resolution attainable by DCS using GS. Actually, a meticulous optimization of the switching and injection conditions is required to produce 1 GHz combs for DCS. Below the gigahertz range, the highest frequency resolution achieved with DCS based on GS and OI reported so far is 500 MHz [16]. However, we have recently demonstrated [17] that the limitation on the line spacing is overcome by a combination of OI and GS with pulsed electrical excitation. In that work, we reported on the generation of flat low-noise combs in the C-band with an optical bandwidth of 85 GHz and a line spacing of 100 MHz. That optical bandwidth has been subsequently broadened to 90 GHz and 112 GHz when the pulsed GS is driven by a low-cost step recovery diode and a pulse pattern generator (PPG), respectively [18]. These results point out the potential of OFCs based on GS with pulsed excitation to perform DCS with high frequency sampling. In this paper, we demonstrate it through the generation of a couple of 100 MHz OFCs based on GS driven by PPGs. By slightly detuning the repetition rate of the driving trains of pulses, we implement a dual-comb system capable of producing ~350 mutually coherent optical lines. That number is comparable to the one achieved by electro-optic dual-comb systems based on external nonlinear broadening [34,35] or non-conventional driving schemes [36]. Our results are also similar to those obtained with two acousto-optic frequency-shifting loops, although without the need of feedback stabilization schemes [37]. The performance of our dual-comb system is comprehensively analyzed by testing different detection schemes and by analyzing the signal-to-noise ratio (SNR) when averaging is carried out.

2. Experimental setup

The experimental setup is shown in Fig. 1. Two OFCs are generated by gain-switching a couple of similar high-frequency distributed feedback (DFB) lasers (Gooch & Housego AA0701 series), both without built-in optical isolator in order to allow external OI. The lasers are driven using the superposition of two electrical signals: a bias current (I_{bias}) and a low duty cycle square signal with peak to peak amplitude V_{pp} and pulse width t_{pulse}. Two PPGs (Anritsu MU181020A) produce trains of square pulses at slightly different repetition frequencies f_{R1} and $f_{R2} = f_{R1} + \delta f$,

Optics EXPRESS

respectively. The operating temperature of both lasers is independently adjusted with two temperature controllers (ILX Lightwave LDT-5412) in order to control the detuning with respect to the master laser. Two optical circulators are used to inject the output power from a narrow linewidth tunable laser (Pure Photonics PPCL300), which acts as master laser, into the two gain-switched DFBs, operating as slave lasers (SL 1 and SL 2). Polarization controllers are included in the setup to maximize the coupling between the master and the slave lasers, and an optical attenuator controls the injected power in each laser, P_{inj}. The OFC generated by SL 2 is frequency shifted a value $f_{shift} = 80$ MHz using an acousto-optic modulator (AA Opto-Electronic MT80-IIR30-Fio-PM0). The optical signals coming from each laser are coupled together and then directed either to a reference path or to a gas cell by means of an optical switch. The signal is then amplified with an erbium doped fiber amplifier (EDFA, Amonics AEDFA-13-B-FA) and mixed in a photodiode (New Focus 1014). A third polarization controller maximizes the beating signal.

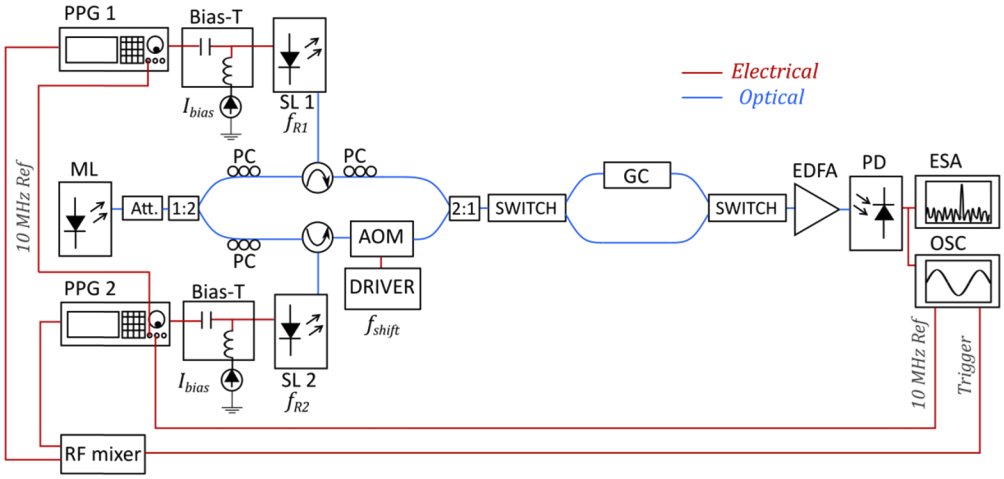

Fig. 1. Experimental setup to perform DCS. In both comb sources, the electrical pulses and the bias signals are coupled to the semiconductor lasers thanks to a bias-tee element (Bias-T). A 10 MHz reference signal generated by one of the PPGs is used as reference for the other PPG and the oscilloscope. The acousto-optic modulator is driven by an independent RF generator (driver). ML: master laser. Att: attenuator. PC: polarization controller. AOM: acousto-optic modulator. GC: gas cell. PD: photodetector. ESA: electrical spectrum analyzer. OSC: oscilloscope.

The gas cell (Wavelength References HCN-13-H(16.5)-25-FCAPC) contains $H^{13}CN$ at a pressure of 25 Torr and its absorption length is 16.5 cm. The P10 line, at 1,549.73 nm, is selected for the measurements. According to the NIST database [38] the normalized transmittance of this line is 0.5592 (absorption depth of 2.52 dB) and according to the manufacturer, its full width at half maximum (FWHM) is around 2 GHz.

In the experiments, the output of the photodiode is measured either with an electrical spectrum analyzer (Agilent E4446A) or, after a proper low-pass filtering, with a real time 20 Gsamples/s digital oscilloscope (Keysight MSOS804A). Note that a digitizer with much lower sampling rate could be employed instead. The trigger for the temporal measurements is obtained by mixing the signals from the two PPGs (taken from the inverted outputs) by means of a RF mixer to get the frequency difference. A common 10 MHz reference is used for the two PPGs and for the oscilloscope. The measurement conditions will be described later together with the results.

In the frequency domain, the interference on the detector of the two frequency combs can be understood as a multi-heterodyne process, in which every line of the first comb beats with

Optics EXPRESS

all the lines of the second comb. If the lower-frequency beat notes (the ones within the first Nyquist zone) are properly filtered, the result is a RF comb that is the down-scaled version of the optical spectrum, with a line spacing δf ($\delta f << f_{R1}, f_{R2}$). Indeed, the bandwidth of the detected signal is the optical one reduced by a compression factor $CF = f_R/\delta f$. The insertion of the acousto-optic modulator in one arm of the interferometer has a twofold purpose. Besides minimizing the influence of the flicker noise, the acousto-optic modulator shift ensures that the beat notes produced by lines symmetrically located around the injection frequency occur at different RF frequencies, thus leading to an unambiguous down-conversion. In the time domain, the detected signal is a sequence of interferograms, each one of duration $1/\delta f$. Figure 1 corresponds to a symmetric or "collinear" dual-comb architecture, since both combs go through the sample. This setup has demonstrated to be very stable and robust, although at the cost of losing phase information. The transmission spectrum is obtained by comparing the Fourier transform of the interferograms produced by the light having passed through the cell with those produced by the light having followed the reference path.

Additionally to the main setup shown in Fig. 1, a digital signal analyzer (Tektronix DSA8200), equipped with a 30 GHz bandwidth optical input module, is employed to measure the temporal profiles of the optical pulses and a 6.25 GHz resolution optical spectrum analyzer (Ando AQ-6315A) is used to measure the optical spectra.

Additional details on the continuous wave (CW) and high-frequency properties of SL 1 and SL 2 can be found in [15]. The threshold currents (I_{th}) and driving conditions of the two slave lasers are summarized in Table 1. Each laser is modulated at the maximum modulation amplitude provided by its corresponding PPG, which is different. As we will show later this difference gives rise to two OFCs with different optical widths.

Table 1. Lasers' driving conditions and modulation parameters

Parameter	SL 1	SL 2
Threshold current I_{th} (mA)	10	11
Bias current I_{bias} (mA)	5.7	9.1
Peak to peak amplitude modulation V_{pp} (V)	2.5	1
Repetition frequency f_R (MHz)	100	100.1
Pulse width t_{pulse} (ps)	200	200
Master laser injected power P_{inj} (dBm)	-11.5	-11.5

The measurement procedure includes the selection of the master laser wavelength at 1,549.63 nm, which is close to, but not equal to the center of the $H^{13}CN$ absorption line (12.5 GHz of detuning), because the combs show instabilities at the injection frequency. The injected power in the slaves is adjusted to ensure injection locking while maintaining broad and flat OFCs [17]. The emission frequencies of the two slave lasers are slightly tuned by temperature in order to have the master laser injection at the blue side of the combs.

3. Results and discussion

3.1. Dual-comb generation

In [17] we investigated the optimal conditions for the generation of OFCs with repetition frequencies of 100 MHz by pulse-driven GS of optically injected laser diodes. Following that analysis, here we generate a couple of OFCs to perform DCS. For this purpose, two PPGs generate trains of electrical pulses with repetition rates of 100 MHz and 100.1 MHz, respectively (δf = 100 kHz), yielding a CF = 1,000. In both cases, the excitation pulses have a nominal duration of 200 ps, which corresponds to a duty cycle of 2%. Figure 2(a) shows the profiles of the pulses measured with the digital signal analyzer mentioned in Sec. 2. The measured FWHM is 190 ps.

Optics EXPRESS

We also employ the digital signal analyzer to visualize the optical pulses generated at the output of each comb source (OFC 1 and OFC 2), which are shown in Fig. 2(b). The FWHM is 43 ps for OFC 1 and 61 ps for OFC 2. This difference is due to the different amplitudes of the electrical pulses applied to the slave lasers. The slaves are switched off most of the time, and because of that, the OI plays a fundamental role in the comb generation, since photons externally injected by the master laser are acting as seed for the growth of new GS pulses when the lasers are switched on again. In that way, coherent emission is guaranteed, leading to the generation of well-resolved optical lines in the frequency domain.

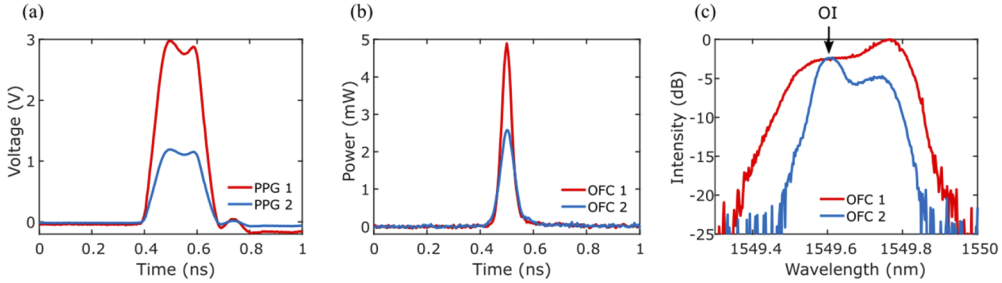

Fig. 2. (a) Electrical pulses produced by the two PPGs to gain switch the lasers, measured with a digital signal analyzer. (b) Temporal profiles of the optical pulses generated by the two slave lasers that produce the individual combs (OFC 1 and OFC 2) measured with a digital signal analyzer placed after the circulators shown in Fig. 1. (c) Optical spectra of both combs displayed in an optical spectrum analyzer with 6.25 GHz of frequency resolution.

The optical spectra of the two OFCs are shown in Fig. 2(c). Due to the limited frequency resolution of the optical spectrum analyzer employed, the comb spectra cannot be resolved line by line. However, the measured envelope allows us to check their flatness and optical bandwidth. In consistency with the time domain measurements, the bandwidth of OFC 2 (~35 GHz within 10 dB) is lower than the one of OFC 1 (~50.5 GHz within 10 dB). Assuming a complete mutual coherence between both combs, the maximum number of optical lines (spaced by 100 MHz) that can be employed in our dual-comb system is around 350 lines, which is more than enough for the spectroscopic measurements considered here. Both combs are appreciably flat, especially OFC 1 (324 teeth within 3 dB). The generation of a flat-topped OFC is achieved by adjusting the power injected into the slave laser and by controlling the point of the GS spectrum where the OI is applied. To do so, each OFC is monitored with the optical spectrum analyzer, while the master laser frequency is finely tuned to guarantee lock-in and to optimize the flatness of the spectra.

The interference of the two OFCs shown before produces time domain interferograms such as the ones depicted in Fig. 3(a), which have a periodicity of 10 µs (the inverse of δf = 100 kHz). By means of the Fourier transform, these interferograms give rise to a down-converted RF spectrum as the one shown in Fig. 3(b). This RF comb is the result of frequency averaging 2,000 spectra, each one retrieved from a temporal trace with a duration of 500 µs (i.e., containing 50 consecutive interferograms). The set of temporal signals is sequentially recorded using the oscilloscope with a sampling rate of 400 Msamples/s. The highest Nyquist zones are filtered out by limiting the oscilloscope bandwidth to 100 MHz. The power spectral density (PSD) of the averaged spectra can be observed in Fig. 3(b). The highest peak located at 80 MHz (the frequency at which the acousto-optic modulator is driven) corresponds to the OI of the master laser. As mentioned before, our dual-comb system produces a flatted-top RF comb (~300 lines within 10 dB, excluding the injection peak). A zoom-in view of this spectrum is shown in Fig. 3(c).

Optics EXPRESS

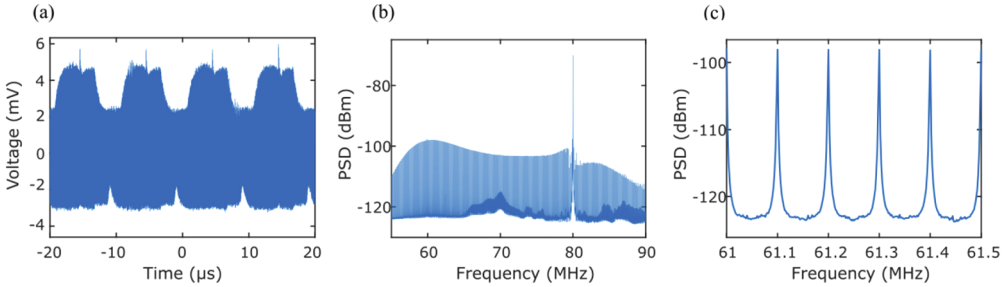

Fig. 3. (a) Time domain interferograms digitized with an oscilloscope. (b) Down-converted dual-comb spectrum obtained from the interferograms retrieved with an oscilloscope. Two thousand spectra, each with a recording time of 500 μs, are averaged (integration time of 1 s). A zoom-in on a few comb lines is shown in (c).

3.2. *Molecular spectroscopy results*

We illustrate the capabilities of our dual-comb system by performing high-resolution spectroscopy with the $H^{13}CN$ gas cell described in Sec. 2. The spectroscopic measurements are carried out by two procedures: from a set of temporal traces digitized by the oscilloscope (fast measurement) and from the electrical spectra acquired with the electrical spectrum analyzer (slow measurement). In Fig. 4 we show three experimental dual-comb molecular spectra measured by means of the oscilloscope for different integration times (t_{int}) to illustrate the evolution of the noise floor with averaging: 1 ms (a), 10 ms (b) and 1 s (c). For these measurements, the switches of our system are configured to make the light propagate through the sample and the presence of an absorption line becomes evident, where the transmission minimum occurs at ~68 MHz. The dual-comb spectrum shown in Fig. 4(c) is retrieved from a sequence of two thousand 500 μs traces, as those from Figs. 3(b) and (c).

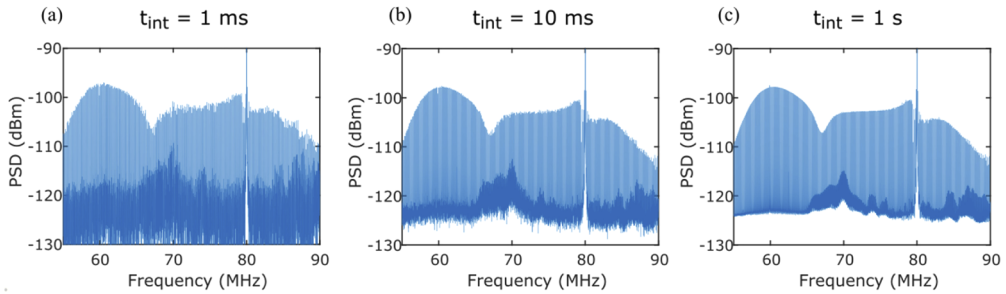

Fig. 4. Down-converted RF combs measured with the oscilloscope when the light goes through the $H^{13}CN$ cell for three different integration times: 1 ms (a), 10 ms (b) and 1 s (c). The vertical scale is reduced to magnify the view of the spectra (the injection peak had an amplitude of ~-70 dBm).

When we analyze the output of the photodetector with the electrical spectrum analyzer, we consider a span of 32 MHz (from 55 MHz to 87 MHz). This frequency interval contains the first Nyquist zone of the RF spectrum generated by dual-comb interference. In order to ensure that the frequency resolution is sufficient to resolve the comb teeth, the number of points is set to its maximum value (8192 points) and the resolution bandwidth is 11 kHz. With this configuration, the sweep time is 1 s, which is the minimum integration time that we can obtain with this method. With the averaging performed by the instrument itself, we achieve integration times up to 2 minutes, which corresponds to 120 averages. Since the electrical spectrum analyzer provides the

Optics EXPRESS

PSD, no further post-processing of the signal is necessary. By normalizing with the reference measurement, and after applying a linear baseline correction, we retrieve the transmission curve. In Fig. 5 we show the transmission profile of the P10 line obtained for integration times of (a) 1 s (1 average), (b) 10 s (10 averages) and (c) 1 minute (60 averages). We show a span of 10 GHz around the absorption peak. In addition, a Voigt profile is fitted to the measured data and the residuals of this fitting process can be observed in the bottom part of each figure. For the last measurement [Fig. 5(c)], the absorption depth and the linewidth provided by the fit are T = 0.56 and FWHM = 2.3 GHz, respectively. These values are in good agreement with the transmission data provided by the NIST [38] and the linewidth specification given by the gas cell manufacturer. For this case (t_{int} = 60 s) the standard deviation of the residuals, σ_{res}, calculated in the 10 GHz span is 0.78 %.

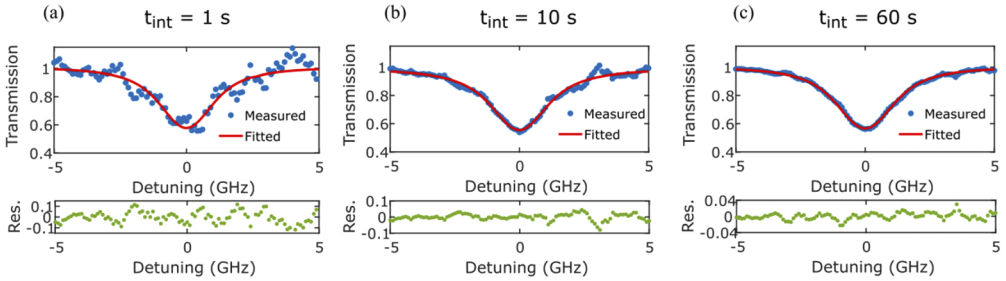

Fig. 5. Transmission profiles obtained from the traces retrieved with the electrical spectrum analyzer, for different acquisition times: (a) 1 s, (b) 10 s and (c) 60 s. A Voigt profile is fitted to the measured transmittances. The corresponding residuals from each fitting process are indicated in the lower part of the figures.

On the other hand, with the oscilloscope we achieve fast measurements, from 500 µs up to 1 s. Traces of 500 µs duration are digitized. Each shot contains 200,000 samples (sampled at 400 Msamples/s), which make up the 50 interferograms contained in each measurement. Thus, to achieve a time of 1 s, 2,000 traces of 500 µs are averaged in the frequency domain. The results of these experiments are illustrated in Fig. 6, for three integration times: (a) 1 ms, (b) 10 ms and (c) 1 s. The corresponding transmission value at the minimum transmission point and FWHM for case (c) are T = 0.54, FWHM = 2.2 GHz. The residuals, shown in the lower part of the figures, do not show systematic deviations. The standard deviation of the residuals for the last integration time (1 s) is σ_{res} = 0.31 %.

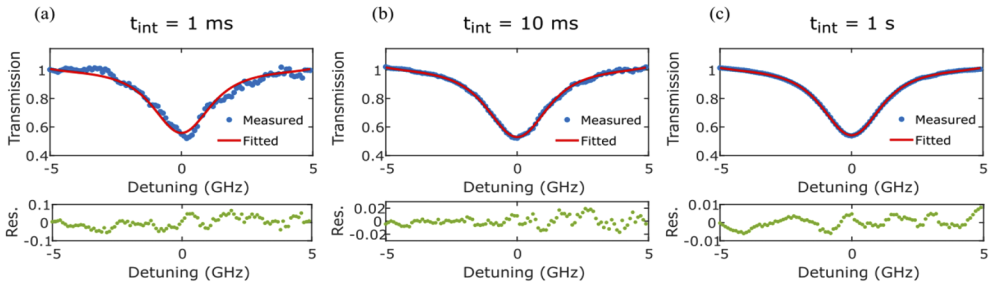

Fig. 6. Transmittances obtained from the temporal data acquired with the oscilloscope for different integration times: (a) 1 ms, (b) 10 ms and (c) 1 s. As in the previous figure, the residuals obtained from the Voigt fitting are shown in the bottom part of each plot.

We analyze the performance of our dual-comb system by means of the product of the SNR and the number of comb lines, M [28]. We calculate the SNR as $1/\sigma_{res}$, being σ_{res} the standard

Optics EXPRESS

deviation of the fitted residuals in a 10 GHz window centered at the transmission minimum. Considering the total number of lines, M = 350, the figure of merit for 1 s of integration time takes values of 1.1×10^5 Hz$^{1/2}$ and 6.3×10^3 Hz$^{1/2}$, for the oscilloscope and electrical spectrum analyzer measurements, respectively. The former value is comparable to previously reported ones [24,39]. The low value of SNR $\times M$ obtained with the electrical spectrum analyzer is a consequence of the operation mode of this instrument, which uses the equivalent to a tunable bandpass filter for selecting the frequency (the resolution bandwidth) disregarding much of the input power during the measurement. If the SNR is computed by dividing the amplitude of a tooth by the average noise between two teeth [40] we obtain a value similar to $1/\sigma_{res}$.

Figure 7 shows the evolution of the quality factor SNR $\times M$ with the integration time for our two acquisition methods. In the case of the oscilloscope, SNR $\times M$ scales in proportion to $\sqrt{t_{int}}$ up to 100 ms and then the slope decreases showing a trend towards saturation at 1 s. In the case of the electrical spectrum analyzer, the value SNR $\times M$ improves also according to $\sqrt{t_{int}}$ from 1 s up to 80 s, with a clear saturation for longer integration times. This improvement of the SNR up to 80 s indicates a very good degree of stability and coherence in our setup.

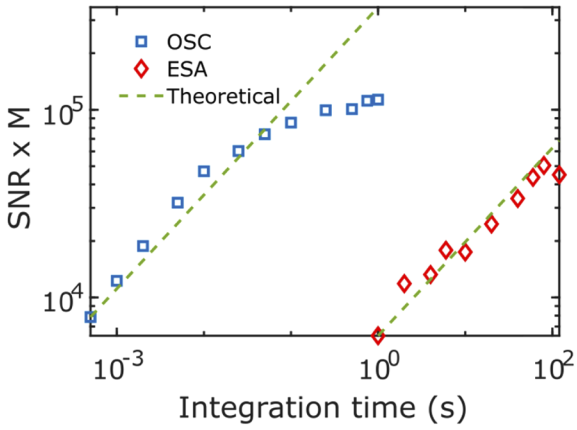

Fig. 7. Quality factor SNR $\times M$ obtained by two acquisition procedures, oscilloscope (blue) and electrical spectrum analyzer (red) for integration times from 500 µs to 120 s. The theoretical evolution of SNR $\times M$ with the integration time (proportional to $\sqrt{t_{int}}$) is indicated for both cases with a green dashed line.

4. Conclusion

In this paper, we have demonstrated a dual-comb system that combines pulsed GS and OI to perform spectroscopy measurements with a frequency spacing of 100 MHz. Our system is capable of producing two mutually coherent combs with M ~350 lines (within 10 dB), thus covering ~35 GHz of optical bandwidth. As is inherent in DCS, this optical bandwidth can be measured with a slow-speed digitizer, thanks to a very efficient frequency down-conversion into the RF domain. The CF in our system is 1,000, so in principle RF bandwidths of only tens of megahertz are involved. We have tested our dual-comb scheme by using a commercial H^{13}CN gas cell. Experimental RF spectra have been retrieved from low-pass filtered and digitized photocurrents. To check their consistency, these spectra have also been directly measured with an electrical spectrum analyzer. In both cases, the retrieved H^{13}CN absorption line is in good agreement with the data found in the literature [38]. By averaging consecutive measurements, in order to increase the SNR, we have achieved a figure of merit SNR $\times M$ (at 1 second) comparable to that previously reported for dual-comb spectrometers generated from CW lasers [24,39]. The measured SNR also shows the expected evolution with the averaging time up to hundreds of

Optics EXPRESS

milliseconds for the oscilloscope measurements and up to tens of seconds in the case of the electrical spectrum analyzer. It should be noted that the line spacing of 100 MHz is more than enough for the spectroscopic measurement presented here. However, the pulsed GS could be easily adjusted to generate frequency combs with a line spacing at least one order of magnitude lower, a performance that could be interesting for applications such as atomic spectroscopy or fiber sensing [41,42]. For spectroscopic measurements requiring a broader optical bandwidth, other techniques and architectures could be implemented, as detailed later on this section, at the cost of increasing the price, complexity and size of the system.

In conclusion, the line spacing of DCS systems based on gain-switched semiconductor lasers can be significantly reduced, so they can be applied to high-resolution spectroscopy, while keeping advantages such as low cost, easy implementation and suitability for photonic integration [43]. In addition, our approach opens up new prospects for further developments. By means of active stabilization or self-correction algorithms [44], averaging times far beyond one second could be achieved. The implementation of comb generators with several stages could lead to expand the attainable optical bandwidth or, alternatively, to densify the generated spectra [45,46]. The number of comb lines could be also incremented by spectral broadening in highly nonlinear fibers [12,47]. On the other hand, increasing the frequency resolution while keeping a high measurement speed could be accomplished by using two combs with dissimilar line spacing [48]. The use of step recovery diodes to generate the electrical pulses [18] and a simpler digitizer for the acquisition of the interferograms, would reduce the complexity and cost of the electronics. Moreover, the integration of the optical part in a photonic circuit would make the solution more cost-efficient and would significantly reduce the footprint of the system. Finally, our dual-comb system could be extended to applications other than spectroscopy, such as laser ranging, in which reducing the comb spacing provides a longer ambiguity range [49].

Funding

European Regional Development Fund/Ministerio de Economía y Competitividad–Agencia Estatal de Investigación (RTI2018-094118-B-C21, RYC-2017-23668); Universitat Jaume I (UJI-B2019-45); Generalitat Valenciana (PROMETEO/2020/029); European Regional Development Fund/Comunidad de Madrid (P2018/NMT-4326); Comunidad de Madrid/Universidad Politécnica de Madrid (APOYO-JOVENES-KXHJ8C-16-VCKM78).

Disclosures

The authors declare no conflicts of interest.

References

1. H. R. Telle, G. Steinmeyer, A. E. Dunlop, J. Stenger, D. H. Sutter, and U. Keller, "Carrier-envelope offset phase control: A novel concept for absolute optical frequency measurement and ultrashort pulse generation," Appl. Phys. B **69**(4), 327–332 (1999).
2. D. J. Jones, S. A. Diddams, J. K. Ranka, A. Stentz, R. S. Windeler, J. L. Hall, and S. T. Cundiff, "Carrier-Envelope Phase Control of Femtosecond Mode-Locked Lasers and Direct Optical Frequency Synthesis," Science **288**(5466), 635–639 (2000).
3. A. Apolonski, A. Poppe, G. Tempea, C. Spielmann, T. Udem, R. Holzwarth, T. W. Hänsch, and F. Krausz, "Controlling the Phase Evolution of Few-Cycle Light Pulses," Phys. Rev. Lett. **85**(4), 740–743 (2000).
4. N. R. Newbury, "Searching for applications with a fine-tooth comb," Nat. Photonics **5**(4), 186–188 (2011).
5. I. Coddington, W. C. Swann, and N. R. Newbury, "Coherent Multiheterodyne Spectroscopy Using Stabilized Optical Frequency Combs," Phys. Rev. Lett. **100**(1), 013902 (2008).
6. P. Marin-Palomo, J. N. Kemal, M. Karpov, A. Kordts, J. Pfeifle, M. H. P. Pfeiffer, P. Trocha, S. Wolf, V. Brasch, M. H. Anderson, R. Rosenberger, K. Vijayan, W. Freude, T. J. Kippenberg, and C. Koos, "Microresonator-based solitons for massively parallel coherent optical communications," Nature **546**(7657), 274–279 (2017).
7. E. Obrzud, M. Rainer, A. Harutyunyan, M. H. Anderson, J. Liu, M. Geiselmann, B. Chazelas, S. Kundermann, S. Lecomte, M. Cecconi, A. Ghedina, E. Molinari, F. Pepe, F. Wildi, F. Bouchy, T. J. Kippenberg, and T. Herr, "A microphotonic astrocomb," Nat. Photonics **13**(1), 31–35 (2019).

Optics EXPRESS

8. I. Coddington, W. C. Swann, L. Nenadovic, and N. R. Newbury, "Rapid and precise absolute distance measurements at long range," Nat. Photonics **3**(6), 351–356 (2009).
9. V. Torres-Company and A. M. Weiner, "Optical frequency comb technology for ultra-broadband radio-frequency photonics," Laser Photonics Rev. **8**(3), 368–393 (2014).
10. A. Parriaux, K. Hammani, and G. Millot, "Electro-optic frequency combs," Adv. Opt. Photonics **12**(1), 223–287 (2020).
11. V. Durán, H. G. de Chatellus, C. Schnebélin, K. Nithyanandan, L. Djevarhidjian, J. Clement, and C. R. Fernández-Pousa, "Optical Frequency Combs Generated by Acousto-Optic Frequency-Shifting Loops," IEEE Photonics Technol. Lett. **31**(23), 1878–1881 (2019).
12. P. M. Anandarajah, R. Maher, Y. Q. Xu, S. Latkowski, J. O'Carroll, S. G. Murdoch, R. Phelan, J. O'Gorman, and L. P. Barry, "Generation of Coherent Multicarrier Signals by Gain Switching of Discrete Mode Lasers," IEEE Photonics J. **3**(1), 112–122 (2011).
13. R. Zhou, S. Latkowski, J. O'Carroll, R. Phelan, L. P. Barry, and P. Anandarajah, "40 nm wavelength tunable gain-switched optical comb source," Opt. Express **19**(26), B415–B420 (2011).
14. H. Zhu, R. Wang, T. Pu, P. Xiang, J. Zheng, and T. Fang, "A novel approach for generating flat optical frequency comb based on externally injected gain-switching distributed feedback semiconductor laser," Laser Phys. Lett. **14**(2), 026201 (2017).
15. A. Rosado, A. Pérez-Serrano, J. M. G. Tijero, Á. Valle, L. Pesquera, and I. Esquivias, "Experimental study of optical frequency comb generation in gain-switched semiconductor lasers," Opt. Laser Technol. **108**, 542–550 (2018).
16. B. Jerez, P. Martín-Mateos, E. Prior, C. de Dios, and P. Acedo, "Gain-switching injection-locked dual optical frequency combs: characterization and optimization," Opt. Lett. **41**(18), 4293–4296 (2016).
17. A. Rosado, A. Pérez-Serrano, J. M. G. Tijero, Á. Valle, L. Pesquera, and I. Esquivias, "Enhanced optical frequency comb generation by pulsed gain-switching of optically injected semiconductor lasers," Opt. Express **27**(6), 9155–9163 (2019).
18. A. Rosado, E. P. Martin, A. Pérez-Serrano, J. M. G. Tijero, I. Esquivias, and P. M. Anandarajah, "Optical frequency comb generation via pulsed gain-switching in externally-injected semiconductor lasers using step-recovery diodes," Opt. Laser Technol. **131**, 106392 (2020).
19. R. Zhou, T. N. Huynh, V. Vujicic, P. M. Anandarajah, and L. P. Barry, "Phase noise analysis of injected gain switched comb source for coherent communications," Opt. Express **22**(7), 8120–8125 (2014).
20. M. D. G. Pascual, V. Vujicic, J. Braddell, F. Smyth, P. M. Anandarajah, and L. P. Barry, "InP photonic integrated externally injected gain switched optical frequency comb," Opt. Lett. **42**(3), 555–558 (2017).
21. M. Imran, P. M. Anandarajah, A. Kaszubowska-Anandarajah, N. Sambo, and L. Potí, "A Survey of Optical Carrier Generation Techniques for Terabit Capacity Elastic Optical Networks," IEEE Commun. Surv. Tutorials **20**(1), 211–263 (2018).
22. J. Pfeifle, V. Vujicic, R. T. Watts, P. C. Schindler, C. Weimann, R. Zhou, W. Freude, L. P. Barry, and C. Koos, "Flexible terabit/s Nyquist-WDM super-channels using a gain-switched comb source," Opt. Express **23**(2), 724–738 (2015).
23. Á. R. Criado, C. de Dios, E. Prior, G. H. Döhler, S. Preu, S. Malzer, H. Lu, A. C. Gossard, and P. Acedo, "Continuous-Wave Sub-THz Photonic Generation With Ultra-Narrow Linewidth, Ultra-High Resolution, Full Frequency Range Coverage and High Long-Term Frequency Stability," IEEE Trans. Terahertz Sci. Technol. **3**(4), 461–471 (2013).
24. B. Jerez, P. Martín-Mateos, E. Prior, C. de Dios, and P. Acedo, "Dual optical frequency comb architecture with capabilities from visible to mid-infrared," Opt. Express **24**(13), 14986–14994 (2016).
25. S. Chandran, S. Mahon, A. A. Ruth, J. Braddell, and M. D. Gutiérrez, "Cavity-enhanced absorption detection of H2S in the near-infrared using a gain-switched frequency comb laser," Appl. Phys. B **124**(4), 63 (2018).
26. A. Rosado, A. Pérez-Serrano, J. M. G. Tijero, A. V. Gutierrez, L. Pesquera, and I. Esquivias, "Numerical and Experimental Analysis of Optical Frequency Comb Generation in Gain-Switched Semiconductor Lasers," IEEE J. Quantum Electron. **55**(6), 1–12 (2019).
27. H. Shams, P. M. Anandarajah, P. Perry, and L. P. Barry, "Optical Generation of Modulated Millimeter Waves Based on a Gain-Switched Laser," IEEE Trans. Microwave Theory Tech. **58**(11), 3372–3380 (2010).
28. I. Coddington, N. Newbury, and W. Swann, "Dual-comb spectroscopy," Optica **3**(4), 414–426 (2016).
29. T. Ideguchi, T. Nakamura, Y. Kobayashi, and K. Goda, "Kerr-lens mode-locked bidirectional dual-comb ring laser for broadband dual-comb spectroscopy," Optica **3**(7), 748–753 (2016).
30. J. Fellinger, A. S. Mayer, G. Winkler, W. Grosinger, G.-W. Truong, S. Droste, C. Li, C. M. Heyl, I. Hartl, and O. H. Heckl, "Tunable dual-comb from an all-polarization-maintaining single-cavity dual-color Yb:fiber laser," Opt. Express **27**(20), 28062–28074 (2019).
31. S. M. Link, A. Klenner, M. Mangold, C. A. Zaugg, M. Golling, B. W. Tilma, and U. Keller, "Dual-comb modelocked laser," Opt. Express **23**(5), 5521–5531 (2015).
32. S. M. Link, D. J. H. C. Maas, D. Waldburger, and U. Keller, "Dual-comb spectroscopy of water vapor with a free-running semiconductor disk laser," Science **356**(6343), 1164–1168 (2017).
33. J. Nürnberg, C. G. E. Alfieri, Z. Chen, D. Waldburger, N. Picqué, and U. Keller, "An unstabilized femtosecond semiconductor laser for dual-comb spectroscopy of acetylene," Opt. Express **27**(3), 3190–3199 (2019).
34. G. Millot, S. Pitois, M. Yan, T. Hovhannisyan, A. Bendahmane, T. W. Hänsch, and N. Picqué, "Frequency-agile dual-comb spectroscopy," Nat. Photonics **10**(1), 27–30 (2016).

Optics EXPRESS

35. V. Durán, P. A. Andrekson, and V. Torres-Company, "Electro-optic dual-comb interferometry over 40 nm bandwidth," Opt. Lett. **41**(18), 4190–4193 (2016).
36. A. J. Fleisher, D. A. Long, Z. D. Reed, J. T. Hodges, and D. F. Plusquellic, "Coherent cavity-enhanced dual-comb spectroscopy," Opt. Express **24**(10), 10424–10434 (2016).
37. V. Durán, C. Schnébelin, and H. G. de Chatellus, "Coherent multi-heterodyne spectroscopy using acousto-optic frequency combs," Opt. Express **26**(11), 13800–13809 (2018).
38. S. Gilbert, W. Swann, and C.-M. J. Wang, "Hydrogen Cyanide H13C14N Absorption Reference for 1530 nm to 1565 nm Wavelength Calibration - SRM 2519a," (2005).
39. V. Duran, L. Djevarhidjian, and H. G. de Chatellus, "Bidirectional frequency-shifting loop for dual-comb spectroscopy," Opt. Lett. **44**(15), 3789–3792 (2019).
40. K. Fdil, V. Michaud-Belleau, N. B. Hébert, P. Guay, A. J. Fleisher, J.-D. Deschênes, and J. Genest, "Dual electro-optic frequency comb spectroscopy using pseudo-random modulation," Opt. Lett. **44**(17), 4415–4418 (2019).
41. D. A. Long, A. J. Fleisher, D. F. Plusquellic, and J. T. Hodges, "Multiplexed sub-Doppler spectroscopy with an optical frequency comb," Phys. Rev. A **94**(6), 061801 (2016).
42. X. Yan, X. Zou, W. Pan, L. Yan, and J. Azaña, "Fully digital programmable optical frequency comb generation and application," Opt. Lett. **43**(2), 283 (2018).
43. J. K. Alexander, L. Caro, M. Dernaika, S. P. Duggan, H. Yang, S. Chandran, E. P. Martin, A. A. Ruth, P. M. Anandarajah, and F. H. Peters, "Integrated dual optical frequency comb source," Opt. Express **28**(11), 16900–16906 (2020).
44. N. B. Hébert, V. Michaud-Belleau, J. Deschênes, and J. Genest, "Self-Correction Limits in Dual-Comb Interferometry," IEEE J. Quantum Electron. **55**(4), 1–11 (2019).
45. P. D. Lakshmijayasimha, A. Kaszubowska-Anandarajah, E. P. Martin, P. Landais, and P. M. Anandarajah, "Expansion and phase correlation of a wavelength tunable gain-switched optical frequency comb," Opt. Express **27**(12), 16560–16570 (2019).
46. B. Xu, X. Fan, S. Wang, and Z. He, "Broadband and high-resolution electro-optic dual-comb interferometer with frequency agility," Opt. Express **27**(6), 9266–9275 (2019).
47. E. Prior, C. de Dios, Á. R. Criado, M. Ortsiefer, P. Meissner, and P. Acedo, "Expansion of VCSEL-Based Optical Frequency Combs in the Sub-THz Span: Comparison of Non-Linear Techniques," J. Lightwave Technol. **34**(17), 4135–4142 (2016).
48. N. B. Hébert, S. Boudreau, J. Genest, and J.-D. Deschênes, "Coherent dual-comb interferometry with quasi-integer-ratio repetition rates," Opt. Express **22**(23), 29152–29160 (2014).
49. Z. Zhu and G. Wu, "Dual-Comb Ranging," Engineering **4**(6), 772–778 (2018).

150.128.148.193 {ts '2020-10-23 01:47:56'}